

Thin film synthesis of hybrid ultramicroporous materials (HUMs)- A comparative approach

Jan Warfsmann¹, Begum Tokay^{1,*}, Neil R. Champness^{2,*}

¹ Chemical and Environmental Engineering Department, Faculty of Engineering, University of Nottingham, Nottingham, NG7 2RD, UK

² School of Chemistry, University of Nottingham, Nottingham, NG7 2RD, UK

Keywords: *Metal-organic Frameworks, Films, TIFSIX, TIFSIX films*

*Corresponding authors

Abstract

The thin-film synthesis of the hybrid ultramicroporous material (HUM) TIFSIX-3-Ni on glass substrates are reported for the first time. Several methods of film formation are employed including dip-coating, seeding and secondary growth, vapour-assisted conversion, rapid thermal deposition and in-situ coating. Using the in-situ approach with dimethylformamide as solvent, we were able to grow homogeneous TIFSIX-3-Ni films at relatively low temperatures (85 °C) and short times (5 h) without substrate modification. During this study, we also significantly reduced the TIFSIX powder synthesis time to 15 h.

1. Introduction

CO₂ is best known as the major contributor to the greenhouse effect and global warming and consequently the separation and capture of CO₂ has become a topic of intense research [1-7]. For CO₂ capture and separation, techniques such as amine-scrubbing, have been known for a long time and are highly effective at removing CO₂ from gaseous mixtures [8]. However, the recovery of the absorbent material (aqueous alkylamine solutions) makes the process cost-intensive [9]. The use of porous materials is a promising alternative and various compounds such as zeolites [10], silica [11] and activated carbon [12], have been investigated extensively for the adsorption and purification of CO₂ [13].

Metal-organic frameworks (MOFs), a class of hybrid porous compounds composed of metal atoms or clusters, connected by organic linkers, are a promising alternative. MOFs have a higher synthetic flexibility in terms of morphology and chemical properties in comparison to the porous materials mentioned above. Consequently, numerous MOFs have been investigated in a wide range of applications including the selective adsorption of CO₂, [14]. For selective CO₂ capture and separation the smaller kinetic diameter and larger polarizability of CO₂, when compared to compounds with which it is commonly mixed, advantageous. However, a common approach, which is used to interact with CO₂, is to increase the polarizability of the host MOFs, particularly by introduction of amine groups in the framework, in order to mimic the conditions of the amine scrubbing, in MOFs such as MIL-53(Al)-NH₂ [15] or UiO-66-NH₂ [16] or the utilisation of open-metal sites in MOFs such as HKUST-1 [17] or CPO-27 (also known as MOF-74) [18]. While both types of MOFs, whether containing amine groups and open-metal sites, have shown improved CO₂ capacities and selectivity at low CO₂ pressures (~0.15 bar, the typical CO₂ partial pressure in flue gas) there are severe drawbacks, which make their use in industrial applications problematic. Amine containing MOFs often have lower porosity and thermal stability in comparison with their pristine compounds [19], while MOFs with open-metal sites typically exhibit reduced water stability [20]. Additionally, in

the latter cases water is an effective competitor for the open-metal sites and regeneration of the compounds often leads to a reduction of CO₂-capacity and long-term stability [21].

In response to the above-mentioned challenges, the use of a new class of MOFs has been proposed. These MOFs are termed hybrid ultramicroporous materials (HUMs) [22] due to their pores with an aperture of less than 0.5 nm [23], which is small in comparison to other MOFs (e.g. ZIF-8: 0.9 nm [24] or CPO-27(Zn): 1.1 nm [25]). HUMs are typically made from layers consisting of metal ions e.g., copper(II) [26] or nickel(II) [27] and a bipyridine linker bridged by anionic pillars e.g., hexafluorosilicate (SiF₆⁻) or hexafluorotitanate (TiF₆⁻). Although, most reported HUMs have a primitive cubic topology, the family of HUMs has been further extended using non-octahedral anions such as dichromate [28], tungsten or molybdenum oxides [29], introducing angularity (non-linearity) to the framework structures. The small pore apertures in these hydrophobic HUMs, in combination with the beneficial interactions between the bridging anionic ligands and guest linear molecules such as CO₂ [30], makes them ideal for potential applications e.g., the purification of propene [23] and acetylene [28], direct CO₂ capture from air and flue gases [31-34] and removal of toxic gases [35, 36].

MOFs are in general first prepared as crystalline powders whilst the use of MOFs might be further expanded by the development of thin-films (depending on the application, the term thin-film can refer to film thickness ranging from a few nanometres to a few hundred micrometres) [37-41]. MOF thin-films have been used in applications such as catalysis [33], membranes for continuous gas separation [38] and in sensors [39]. However, the conversion of a powder synthesis to a thin-film synthesis is not a trivial task [41]. The thin-film formation of HUMs has been conducted until now mostly by liquid-phase epitaxy (LPE) [42], a technique, where a support is alternately immersed in metal and linker solution with intermediate removal of weakly attached components in pure solvent. While the LPE approach enables precise control over the film-thickness with atomic resolution [43], the accessible film-thickness of the LPE is in general less than 100 nm, which is not adequate for applications such as membranes for gas separations [44]. However, a recent report showed that creating micron thick films of HUMs by using LPE on porous alumina supports were possible [45]

Amongst the existing HUMs, TIFSIX-3-Ni {[Ni(pyrazine)₂(TiF₆)]_n, referred as TIFSIX from now on} [46] was chosen as one of the most promising candidates. In TIFSIX, the nickel atom is surrounded by 4 pyrazine groups through Ni-N bonds, leading to the formation of a cubic primitive cell. The two remaining octahedral positions around the metal atoms are occupied by TiF₆²⁻-anions, separating the layers composed of nickel and pyrazine. It has a very similar structure to the silicon derivative, SIFSIX-Ni, for which a crystal structure has been already published [27] (Figure 1). However, the shorter length of the Ti-F bond in comparison to Si-F leads to a pore aperture of ~0.35 nm in TIFSIX [42], which is close to the kinetic diameter of CO₂ (~0.33 nm [48]). This, in turn, leads to one of the highest known CO₂ adsorption capacity (~40 cm³ g⁻¹ at 2 mbar CO₂ pressure) for a MOF [46], and selectivity at low CO₂ pressures. Moreover, the synthesis of TIFSIX does not rely on expensive starting materials or toxic hydrofluoric acid.

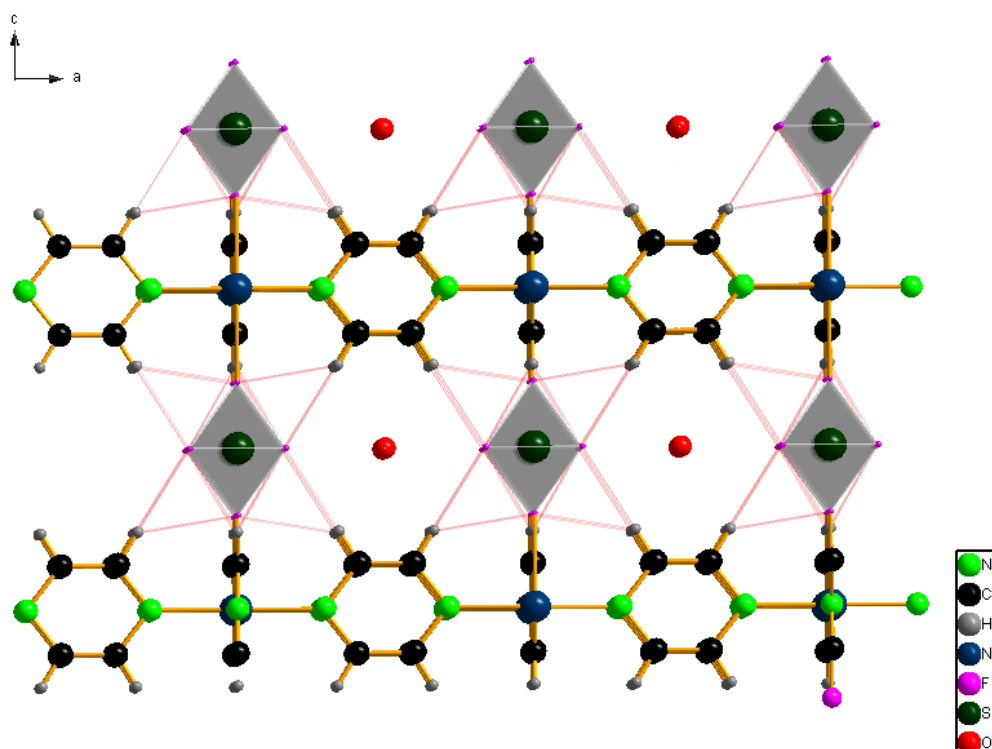


Figure 1: Structure of the derivate SIFSIX-3-Ni, which is isostructural to TIFSIX-3-Ni. The structure was calculated from existing crystal data [27]. The oxygen (red) in the pores represent water bound in the pores before activation. Bonds in red highlight stabilization of the framework by H-F bonds.

Herein, we present the thin-film formation of TIFSIX by a straightforward in-situ synthesis on a glass support without the need for pre-emptive surface modification. In this study, we show the first example of preparation of TIFSIX films on glass substrates using various film synthesis strategies. We employ strategies including dip-coating, seeding and secondary growth, vapour-assisted conversion, rapid thermal deposition and in-situ coating. Amongst those methods used, only seeding and secondary growth and in-situ coating methods resulted in the formation of TIFSIX films with thicknesses of a few microns on glass substrates.

2. Experimental

2.1 Materials

Nickel carbonate basic hydrate ($\text{NiCO}_3 \cdot 2\text{Ni}(\text{OH})_2 \cdot 4\text{H}_2\text{O}$), pyrazine and hexafluorotitanic acid (H_2TiF_6 , 60 wt% in water) were purchased from Sigma Aldrich. The solvents *N,N*-dimethylformamide (DMF), acetone and methanol (MeOH) were purchased from Fischer Scientific. All chemicals were reagent grade and used as received. Deionised water was collected from Millipore Direct-Q 5 UV water purification system.

2.2 Methods

2.2.1 Synthesis of NiTiF_6

In a typical reaction, $\text{NiCO}_3 \cdot 2\text{Ni}(\text{OH})_2 \cdot 4\text{H}_2\text{O}$ (3 g, 4.93 mmol) was added to 15 ml deionised water and the suspension stirred for 15 min at room temperature (RT). H_2TiF_6 (1.5 g as 60% solution in water, 10.98 mmol) was added and the reaction mixture stirred for additional 5 min. The reaction mixture was stored at RT for 2 days. After filtration, the solvent was evaporated for 1 day at 90 °C resulting in a green, highly hygroscopic solid. Drying at 90°C was continued

until a solid green product was formed. After 3 days drying time, 2.152 g (87% yield) of NiTiF_6 was collected.

2.2.2 Synthesis of TIFSIX powder

TIFSIX was prepared using a slightly modified process to the literature procedure [30, 46]. NiTiF_6 (0.5 g, 2.22 mmol) and pyrazine (1 g, 12.48 mmol) were each dissolved in 5 ml of DMF and stirred at RT. After 15 min, the pyrazine solution was added to the NiTiF_6 solution and stirred for additional 15 min. The reaction mixture was poured into a 45 ml Teflon[®]-lined stainless-steel pressure vessel (Parr Instruments 4744 General Purpose Acid Digestion Vessel) and heated to 85 °C. After 15 h reaction, the product was separated by centrifugation at 4000 rpm for 30 min and the solution was decanted. The product was washed with water and activated in MeOH by solvent exchange for in total 3 days. The MeOH was exchanged daily for fresh MeOH. The product was obtained as a purple powder after heating in vacuum at 120 °C for 24 h.

2.2.3 Thin film synthesis methods

2.2.3.1 In-situ

A glass slide (soda-lime microscope slides, Fischer Scientific Menzel Gläser) was cut into pieces with dimensions of 1 x 1 cm, immersed in acetone and cleaned by ultrasonication for 30 min. The glass slide was washed with deionised water and dried in an N_2 -flow. For the in-situ coating, a cleaned glass slide was mounted vertically in a Teflon[®]-lined stainless-steel autoclave with 10 ml of TIFSIX reaction mixture (0.5 g NiTiF_6 and 1g pyrazine in 10 ml DMF) placed in an oven at 85 °C. Reactions were conducted for 1, 5 and 15 h. The vessel was naturally cooled down to RT for 5 h before the glass slide was removed from the vessel. The glass slide was washed with MeOH to remove loose powder, placed in a beaker with 10 ml MeOH for 1 day and dried in an oven at 150 °C for 2 h.

2.2.3.2 Dip-coating

A powder sample of TIFSIX-3-Ni (0.5 g) prepared in DMF was grounded for 10 min with mortar and pestle and added to MeOH (9.95 g). The resulting suspension was placed in an ultrasonic bath for 10 min and then vigorously stirred for 10 min at RT. A cleaned glass slide was immersed into the suspension for 1 min and vertically extracted from the suspension. The glass slide was placed on a petri dish and solvent evaporated for 2 h at 100 °C. To add additional layers, the procedure was repeated as required.

2.2.3.4 Seeding and Secondary-growth

A seeded glass slide, with a thin film prepared using two dip-coating procedures (see 2.2.3.2), was mounted vertically by a Buehler SamplKlip[®] and placed in a Teflon[®]-lined stainless steel autoclave filled with 10 ml of TIFSIX reaction mixture (0.5 g NiTiF_6 and 1 g pyrazine in 10 ml DMF). The reaction vessel was placed in an oven at 85 °C for 15 h. After the reaction, the vessel was slowly cooled to RT (storing at RT for 5 h) and the glass slide removed. Loose powder was removed by washing the glass slide with MeOH from a wash bottle and the sample dried for 17 h at 100 °C.

2.2.3.5 Vapour-Assisted Conversion

A cleaned glass slide was placed for 1 min in TIFSIX reaction mixture in DMF as solvent DMF (0.5 g NiTiF_6 and 1 g pyrazine in 10 ml DMF) vertically extracted and then placed on a grid in a crystallization dish. A porcelain evaporation dish, acting as stand for the grid and reservoir,

was filled with 10 ml DMF and the vessel closed with a petri dish as lid [45]. The closed vessel was placed in oven at 85 °C for 15 h. After removal from the oven, the lid was removed to let excess solvent evaporate from the glass surface for 15 h at RT. Weakly attached sample was removed by MeOH from wash bottle and the sample dried for 17 h at 100 °C.

2.2.3.6 Rapid-Thermal Deposition

The Rapid-Thermal Deposition (RTD) film synthesis was conducted using a slightly modified version of the approach described by Shah et.al [56]. For the RTD film synthesis, a cleaned glass slide was placed for 1 min in TIFSIX reaction mixture (0.5 g NiTiF₆ and 1 g pyrazine in 10 ml DMF), vertically extracted, placed on a petri dish and the reaction conducted at 85 °C for 15 h. After the reaction the glass slide was naturally cooled down to RT (storing for 5 h at RT) and weakly attached sample removed by washing with MeOH from washing bottle. Activation was conducted by solvent exchange in MeOH at RT for 1 day and heated at 100 °C for 1 day.

2.3 Characterisation

Scanning electron microscopy (SEM) was used to characterise the morphology and crystal size, calculated from an average of 25 particles. Measurements were conducted using either a JEOL JSM-7100F Field Emission Gun (FEG) or a JEOL 6490LV instrument. The measurements were conducted with a beam voltage of 15 kV. All samples were sputtered with a 10 nm iridium film by a Quorm Q150T ES coater in order to increase conductivity of the samples.

X-ray diffraction (XRD) measurement was performed using a PANalytical X'Pert Pro diffractometer operating at 40 kV, 40 mA and CuK α radiation (λ : 1.540598 Å), equipped with a PIXCell3D detector. The experiments were conducted in continuous scanning mode with the goniometer fixed in the theta/theta orientation. For the incident site and detector site a soller slit of 0.04 rad° and an incident beam mask of 15 mm was used. The irradiated length was 10.0 mm. In a typical powder experiment ~50 mg of powder sample was used, and scans were conducted in a range of 5-40° 2 θ with a step size of 0.006565° and a scan time of 51 s per step, resulting in a total measurement time of ~17 min. For glass slide samples, the scan time per step was increased to 440 s leading to a total measurement time of ~2 h.

Thermal stability of the powder samples was investigated by TGA using a TA instruments Q500 thermal gravimetric analyser. Samples were heated up to 700 °C under air flow (100 ml min⁻¹) with a heating rate of 5 °C min⁻¹.

CO₂ isotherms were measured using a Micrometrics 3Flex adsorber. During the measurement, the temperature was set at 25°C and the data was collected between 6 and 1013 mbar absolute pressure.

3. Results and Discussions

Previous reports of TIFSIX preparation described synthesis in water or MeOH for reaction times up to 3 days at room temperature [30, 46]. During our investigation, we determined that using DMF as solvent at 85 °C, the reaction time could be significantly reduced to 15 h. The characteristic peaks at 12.5° and 17.8°, shown in the XRD pattern, obtained using our shorter reaction times matches (Figure 2) previously reported XRD patterns [46], after activation by solvent exchange in MeOH and heating at elevated temperature in vacuum. Similarly, TGA analysis of the TIFSIX material matches literature reports [46] (Figure S1).

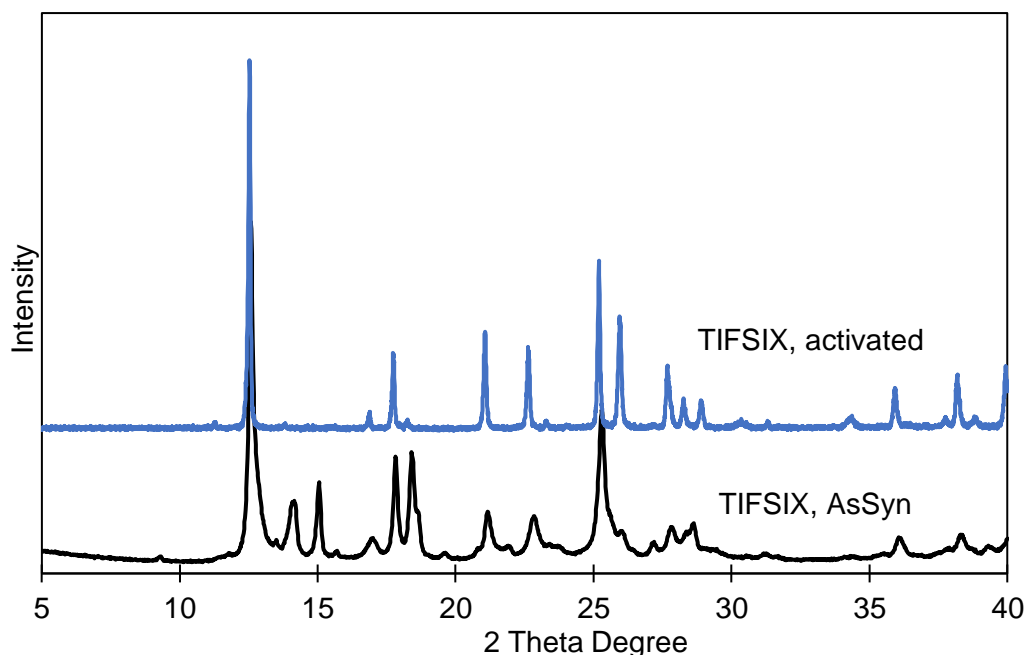


Figure 2: XRD patterns of TIFSIX powder prepared in DMF at 85 °C for 15 h after synthesis (“AsSyn”, black) and after activation by solvent exchange in MeOH and heating at elevated temperature in vacuum (“activated”, blue).

The morphology of the resulting powder sample was investigated by SEM (Figure 3). The needle-shaped particles observed are up to 10 μm long. SEM image at higher magnification confirmed that the needle-shaped particles are fused from nanometre-sized cubic particles. In addition, some larger cubic particles (up to 850 nm) could also be identified in the powder sample (Figure 3b). The synthesis of TIFSIX in DMF at 85 °C was used as the starting point for the further development of thin-film techniques.

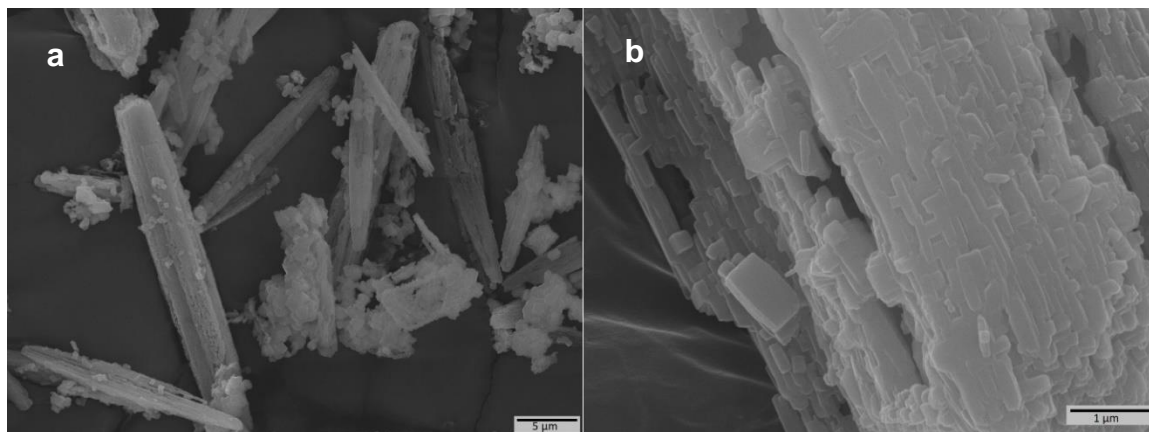


Figure 3: SEM images of TIFSIX powder prepared in DMF at 85 °C for 15 h at lower (a, scale bar: 5 μm) and higher (b, scale bar: 1 μm) magnifications.

For the in-situ coating, the effect of the reaction time on the quality of the thin-film was investigated for 1, 5 and 15 h synthesis times. Figure 4 shows top surface and cross section SEM images of the glass surface after 1 h. The surface is partially covered and large gaps are still visible on the substrate. The cross-section image of the film further shows that the coating has a thickness of approx. 4.8 μm but with gaps in the film (Figure 4).

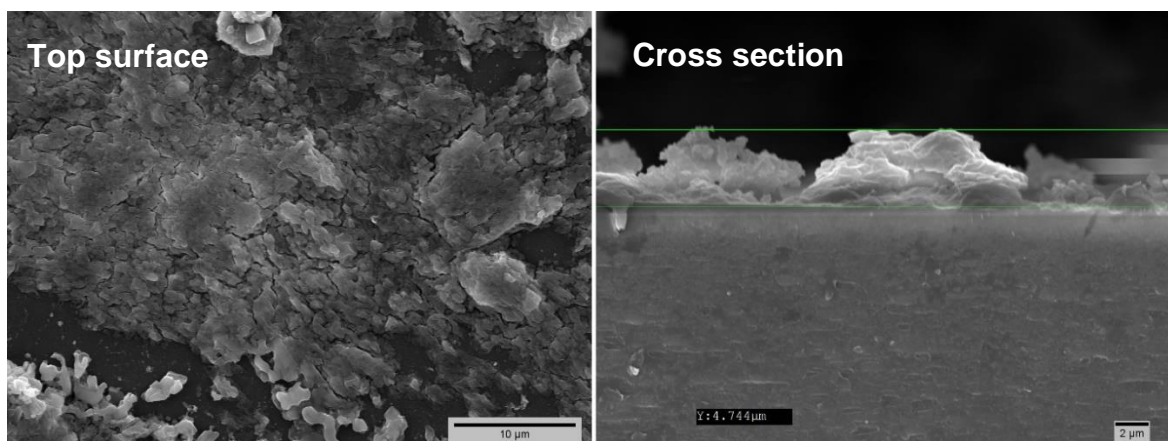


Figure 2: SEM image of top surface and cross-section of glass slide coated with TIFSIX via in-situ coating in DMF at 85 °C for 1 h.

An XRD pattern of the sample (Figure 5) verified the successful coating of the surface with TIFSIX. The peaks positions match the pattern measured from the powder sample, but the intensity is low in comparison to the glass background. We assume that the relative low intensity of the TIFSIX peaks can be attributed to the non-homogenous coating and low surface coverage. In addition, intensity of the characteristic peaks is influenced by crystal orientation and packing density [48, 51]. In our study, we expect that crystals were randomly oriented since we did not attempt to control orientation.

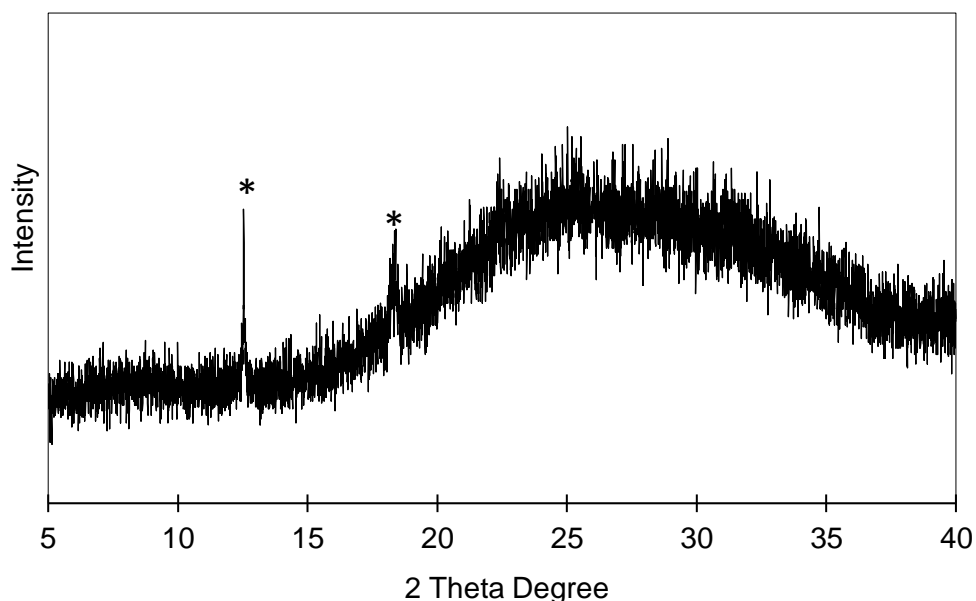


Figure 5: XRD pattern of glass slide coated with TIFSIX via in-situ coating in DMF at 85 °C for 1 h. Peaks matching TIFSIX are highlighted with asterisk.

Although coating the surface of the substrate with TIFSIX film was possible in an hour, the SEM images of the surface showed that this coating was not homogeneous. In contrast, after 5 h reaction time, the surface is homogeneously covered by cubic crystals. The film-thickness is approx. 4.6 μm, similar to the sample prepared in 1 h, but particles are fused. Increasing reaction times to 5 and 15 h led to improved surface coverage. After 5 h, the surface of the glass slide was mostly covered by cubic particles (edge length $\sim 586 \pm 112$ nm) (Figure 6) and

only small gaps in the coating were visible (Figure S2). Similar cubic particles were observed as for the powder sample, agglomeration into needle-shaped particles being seen for the latter case. The size of the cubic particles on the coated surface was comparable to the powder sample (Figure 3). A cross-section of the sample after 5 h showed that the thickness of the coating was homogeneous and smooth, probably caused by fused particles, with a depth of approximately 4.6 μm , comparable to the coating after 1 h (Figure 6).

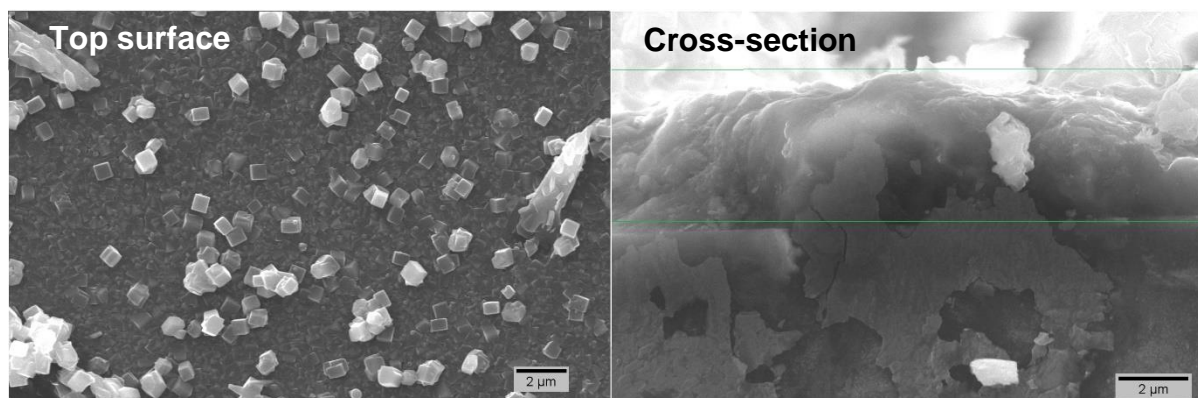


Figure 3: SEM image of top surface and cross-section of glass slide coated with TIFSIX via in-situ coating in DMF at 85 $^{\circ}\text{C}$ for 5 h.

Achieving thin-film synthesis of TIFSIX in a single growth cycle without seeding or modification of glass substrate is significant. Similarly, HKUST-1 [52] and ZIF-8 [53, 54] thin-films were successfully synthesised on glass and quartz substrates without seeds using in-situ growth technique. However, 40 and 5 growth cycles were needed, respectively, in order to grow films with sufficient thickness. In addition, we developed vapour-assisted conversion approach for synthesis of MIL-53 thin-films using seeded substrates (glass and ceramic) since application of many well-known synthesis methods failed to produce films with homogeneous coverage [40].

After 15 h, the surface is completely covered with micron size needle-shaped particles with a film thickness of approx. 6.9 μm (Figure 7). These particles are composed of smaller cubic particles (Figure S3) and resemble the morphology of TIFSIX powders synthesised in DMF. We therefore assume that after shorter reaction times (5 h) the cubic particles did not agglomerate to the larger needle-shaped particles, which are observed after 15 h. The needle-shaped particles may be a combination of agglomerated and fused particles. The cubic particles with clear edges may continue to grow at the edges and after certain reaction times, neighbouring crystals start to fuse forming needles. Change in shape with longer synthesis time may also indicate that the TIFSIX crystals are evolving to a more stable phase. A similar phenomenon was observed for ZIF-8 films where increased reaction times and metal concentration results in spherical ZIF-8 crystals becoming rhombic, which is considered a more stable phase [55]. A cross-section image of the surface showed that the longer reaction times led to a $\sim 6.9 \mu\text{m}$ coating, thicker and rougher than the coating prepared after 5 h (Figure 7). In contrast to the 1 h sample, the surface was completely covered without visible gaps. In addition, for both samples prepared over 5 h or 15 h, films were well attached to the substrate.

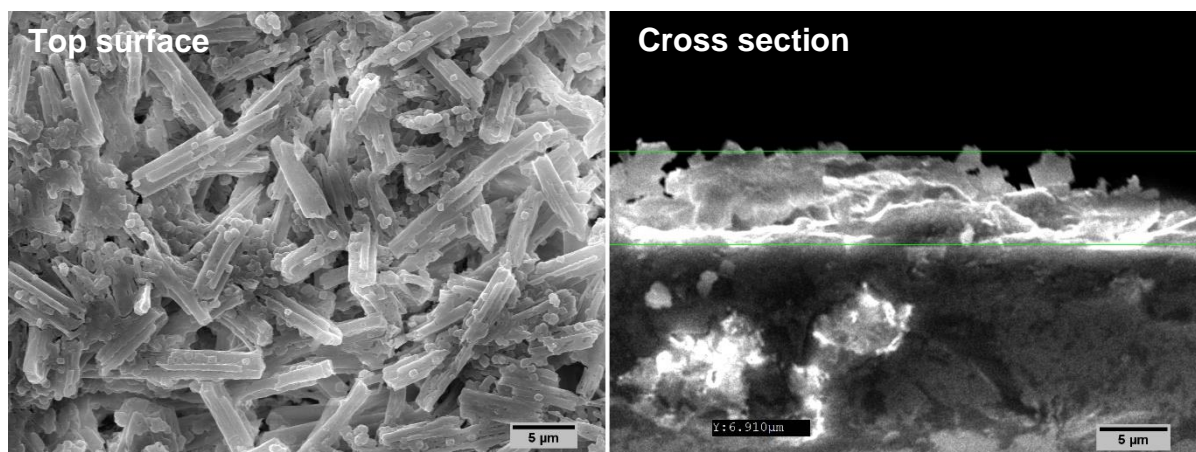


Figure 7: SEM image of top surface and cross-section of glass slide covered with TIFSIX via in-situ coating in DMF at 85 °C for 15 h.

XRD patterns of coatings after 5 or 15 h reaction times exhibit similar patterns with slightly lower intensity of the peaks for the 5 h sample, probably as a result of the thinner coating (Figure 8). Although peaks at 12.6° and 17.8° confirm the successful coating of TIFSIX, additional peaks at 15.7° and 18.2° show that the coatings contain impurities. Similar to the powder synthesis in DMF, these impurities could be mostly removed by solvent exchange in MeOH for 1 day. The XRD pattern (Figure S4) shows that peak at 15.7° could be completely removed and the peak at 18.2° reduced in intensity. We also investigated ultrasonication to speed up the activation process. No weight loss of crystals from the substrate was recorded. There were no new gaps between the crystals were formed. These confirm the strong interaction of the TIFSIX film to the glass surface since no degradation and exfoliation occurred.

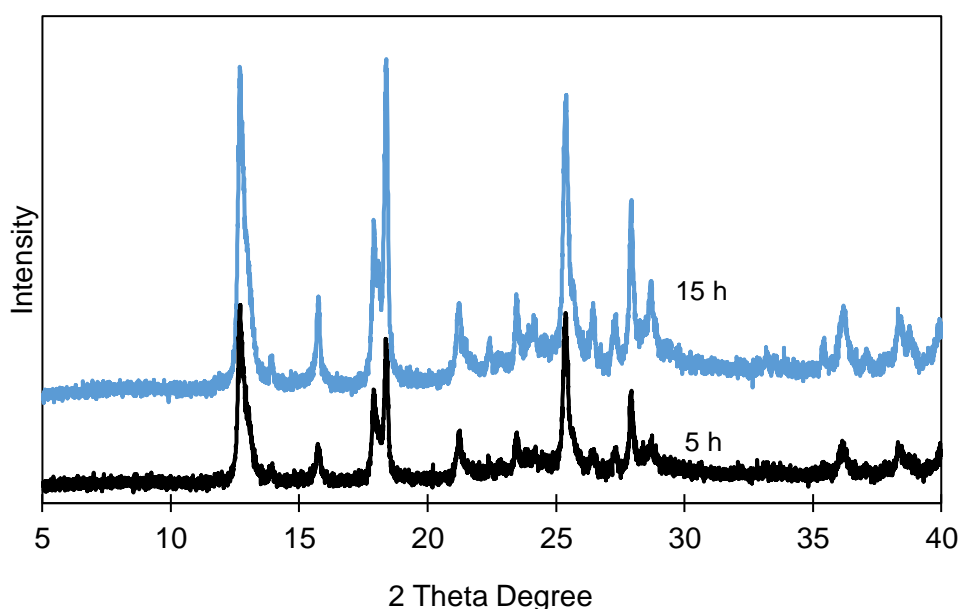


Figure 8: XRD patterns of glass slides covered by TIFSIX in DMF via in-situ coating at 85 °C for 5 and 15 h before activation by solvent exchange.

The CO₂ isotherm of the powder sample, collected from the bottom of the vessel, at the end of the in-situ film formation, shows the porosity of the crystals attached to the surface (Fig S5). Although the CO₂ adsorption capacity of the powder is approx. 20 cm³ g⁻¹, this amount is

sufficient for the detection of ppm level CO₂ using sensors. HUMs such as TIFSIX, are known to have strong selectivity for CO₂ over other gases, including N₂ [46]. This would mean that N₂ is less strongly bound and therefore N₂ isotherms would not be a useful measurement. In addition, N₂ isotherm measurements are less relevant for potential applications.

Figure 9 shows the SEM images of TIFSIX particles attached to the glass slide after one- and two-cycles using dip-coating. The surface was mostly uncovered and only a few spots were coated with particles after one-layer coating. Crystal agglomeration and cracks are also visible. In comparison with the one-layer sample, the coverage was increased after two-layer coating whilst the surface was still mostly uncovered. A further repetition of the dip-coating process or increasing the amount of the powder in the initial suspension might lead to an increase of the surface coverage. However, obtaining homogeneous films of TIFSIX can still be challenging. While no peaks could be identified for the one-layer sample, the peaks of the two-layer sample match the powder pattern of TIFSIX. However, the intensity of the peaks relative to the glass background is low, probably due to a reduced surface coverage (Figure S4). We expected to observe some crystal growth using the dip-coating technique since the TIFSIX crystals, which were mixed with the initial synthesis solution, could promote nucleation and growth. This may suggest that the TIFSIX crystals in the suspension were dissolved while the solvent was evaporated rather than attaching to the glass surface. Although dip-coating conditions were similar to the in-situ method, the solution to provide nutrients was not present, compared to the in-situ method. Therefore, crystals could not grow to form a film via the dip-coating method. In contrast, in a recent publication, Chernikova et.al showed the successful formation of a SIFSIX-3 membrane on a porous alumina support using a similar method [45]. Therefore, obtaining low surface coverage and low intensity of the TIFSIX characteristic peaks in our study may well be due to using glass substrates with a non-porous inert surface.

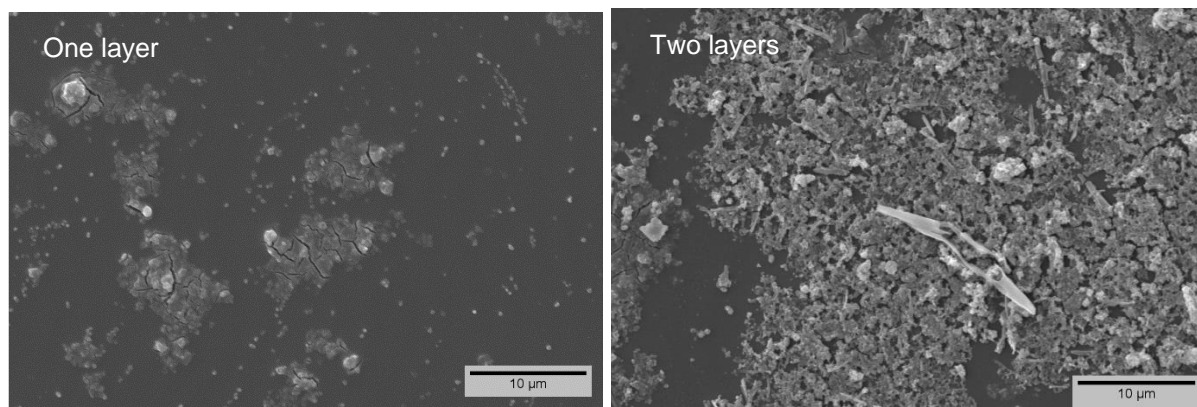


Figure 9: SEM images of glass slides covered with TIFSIX particles by dip-coating after one- and two-layer.

To promote the particle attachment to the glass surface, a seeding and secondary growth approach was employed, which can facilitate formation of homogeneous and crack-free films. We seeded the glass slide by employing dip-coating method on two occasions rather than a bare surface. This approach definitely enabled nucleation and growth of TIFSIX crystals on the glass slide, as shown in Figure 10. Although the surface was almost completely covered, numerous cracks and holes were visible in the coating, in comparison to in-situ coating (Figure 7). Spherical particles are observed with more defined boundaries, which are agglomerated

but not fused, as seen after using the in-situ method. These particles are smaller than those formed via the in-situ method, indicating increased nuclei formation and a fast nucleation rate for the seeding and secondary growth approach. This may suggest that particles are more evolved to their thermodynamically stable state when the in-situ method is employed. The XRD pattern of a glass slide coated with TIFSIX, using the seeding and secondary growth method shows the characteristic peaks at 12.6° and 17.8° . These are attributed to TIFSIX whilst several impurity peaks are also seen, indicating an incomplete activation of the sample. Due to the inhomogeneous coating and absence of fused particles, further investigations (e.g. activation of the sample) were not conducted using this coating technique.

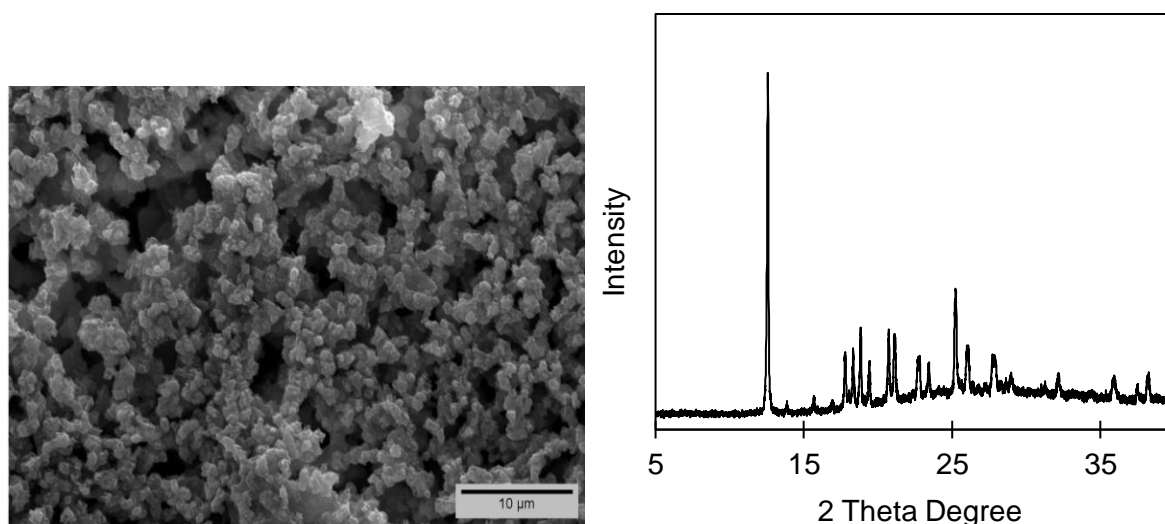


Figure 10: SEM image and XRD pattern of a glass slide covered with TIFSIX particles by seeding and secondary growth.

The other approaches employed in this study, such as synthesis in a saturated solvent atmosphere (VAC [50]) and growth from small films of reaction mixture followed by fast evaporation of the solvent (RTD [56]), seemed to hinder the formation of TIFSIX since the unreacted starting material remained on the surface and yet another unknown material was produced (Fig 11). The peak at 18.7° (highlighted by asterisks, Fig 11a-VAC) can be attributed to the starting material NiTiF_6 (Fig S7), while the other peaks (e.g., at 19.3° and 20.6°) are unknown impurities. Peaks, which can be attributed to TIFSIX, were not observed in the XRD pattern of the film. In contrast, the peaks observed for the films, prepared using RTD technique, are close to the known diffraction pattern of the TIFSIX powder sample [3]. However, the peak at $\sim 18^\circ$ is slightly shifted (18.2° instead of the expected 17.8°) and the relative intensities of the peaks at $\sim 12^\circ$ and $\sim 18^\circ$ do not match the expected diffraction pattern. We assume that rather than the primitive cubic topology of TIFSIX, a material with a square grid topology was formed [49]. Due to the unsuccessful synthesis of TIFSIX, no activation e.g., solvent exchange and heating at elevated temperature, was attempted.

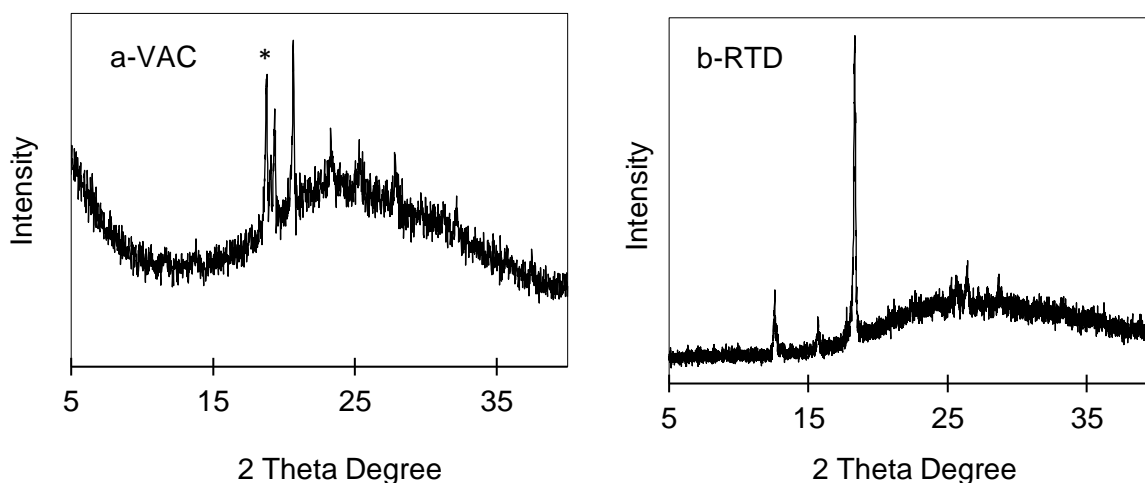


Figure 11: XRD patterns of the glass slides covered by vapour-assisted conversion (VAC) and rapid-thermal deposition (RTD).

The SEM images of the films coated via VAC and RTD methods are shown in Figure S8. After employing the VAC method, the surface is partly covered with particles, but the particles are not intergrown and large gaps can be identified. These particles have a cuboid shape with a length of $1.7 \pm 0.4 \mu\text{m}$ (Fig S8a). Although the film prepared via the RTD method displays some of the characteristic peaks of TIFSIX, the film is not homogenous and cracks are visible (Fig S8b).

4. Conclusions

In conclusion, we have demonstrated the successful preparation of thin-films of TIFSIX using an in-situ coating process at $85 \text{ }^\circ\text{C}$ as short as 1 h. Micron thick coatings fabricated in this study will ensure sensing and separation applications of TIFSIX films, with respect to their high CO_2 selectivity. The in-situ coating approach has an advantage since no additional steps such as substrate modification, is necessary. The morphology and film thickness vary with reaction time. After 5 h, the surface was mostly covered with cubic particles, while the particles are needle-shaped after 15 h. Both reaction times led to the formation of homogenous and crack-free films with well-fused crystals. Although successful coatings of TIFSIX could be confirmed using XRD, the patterns showed several impurities, which could not be completely removed by the activation process. A repetition or modification of the activation process, adopted from the powder synthesis, might be necessary to increase purity of TIFSIX thin-films. Attempts to coat glass substrates with TIFSIX films using dip-coating, rapid-thermal deposition and vapour-assisted conversion were unsuccessful. The surfaces were not homogeneously covered or the samples could not be verified as TIFSIX *via* XRD. We believe that our approach can be used to develop thin-films of other HUMs and for the further application of these fascinating materials.

5. Acknowledgement

This work was supported by the Engineering and Physical Sciences Research Council (EPSRC, EP/L022494/1). NRC thanks the Engineering and Physical Sciences Research Council (EP/S002995/1) for support. JW gratefully acknowledges receipt of a University of Nottingham Research Scholarship. The authors thank the Nanoscale and Microscale Centre

(nmRC) for providing access to instrumentation. We thank Prof. Mike Zaworotko for useful discussions.

6. References

- 1 M. Shah, M. C. McCarthy, S. Sachdeva, A. K. Lee and H.-K. Jeong, *Ind. Eng. Chem. Res.*, 2012, 51, 2179–2199.
- 2 M. Songolzadeh, M. Soleimani, M. Takht Ravanchi and R. Songolzadeh, *The Scientific World Journal*, 2014, 2014, 828131.
- 3 R. S. Haszeldine, *Science*, 2009, 325, 1647–1652.
- 4 A. Phan, C. J. Doonan, F. J. Uribe-Romo, C. B. Knobler, M. O'Keeffe and O. M. Yaghi, *Acc. Chem. Res.*, 2010, 43, 58–67.
- 5 H. Yang, Z. Xu, M. Fan, R. Gupta, R. B. Slimane, A. E. Bland and I. Wright, *J. Environ Sci.*, 2008, 20, 14–27.
- 6 J.-R. Li, Y. Ma, M. C. McCarthy, J. Sculley, J. Yu, H.-K. Jeong, P. B. Balbuena and H.-C. Zhou, *Coordin. Chem. Rev.*, 2011, 255, 1791–1823.
- 7 Y.-S. Bae and R. Q. Snurr, *Angew. Chem. Int. Ed.*, 2011, 50, 11586–11596.
- 8 G. T. Rochelle, *Science*, 2009, 325, 1652–1654.
- 9 D. M. D'Alessandro, B. Smit and J. R. Long, *Angew. Chem. Int. Ed.*, 2010, 49, 6058–6082.
- 10 O. Cheung and N. Hedin, *RSC Adv.*, 2014, 4, 14480–14494.
- 11 L.-Y. Lin and H. Bai, *Micro. Meso. Mat.*, 2010, 136, 25–32.
- 12 M. M. Maroto-Valer, Z. Tang and Y. Zhang, *Fuel Process. Technol.*, 2005, 86, 1487–1502.
- 13 S. Choi, J. H. Drese and C. W. Jones, *ChemSusChem*, 2009, 2, 796–854.
- 14 C. A. Trickett, A. Helal, B. A. Al-Maythaly, Z. H. Yamani, K. E. Cordova and O. M. Yaghi, *Nat. Rev. Mat.*, 2017, 2, 1230444.
- 15 B. Arstad, H. Fjellvåg, K. O. Kongshaug, O. Swang and R. Blom, *Adsorption*, 2008, 14, 755–762.
- 16 M. Kandiah, M. H. Nilsen, S. Usseglio, S. Jakobsen, U. Olsbye, M. Tilset, C. Larabi, E. A. Quadrelli, F. Bonino and K. P. Lillerud, *Chem. Mater.*, 2010, 22, 6632–6640.
- 17 S. S.-Y. Chui, S. M.-F. Lo, J. P. H. Charmant, A. G. Orpen and I. D. Williams, *Science*, 1999, 283, 1148–1150.
- 18 S. R. Caskey, A. G. Wong-Foy and A. J. Matzger, *J. Am. Chem. Soc.*, 2008, 130, 10870–10871.
- 19 X. Y. Chen, V.-T. Hoang, D. Rodrigue and S. Kaliaguine, *RSC Adv.*, 2013, 3, 24266–24279.
- 20 L. Riboldi and O. Bolland, *Energy Proc.*, 2017, 114, 2390–2400.
- 21 A. Kumar, D. G. Madden, M. Lusi, K.-J. Chen, E. A. Daniels, T. Curtin, J. J. Perry, 4th. and M. J. Zaworotko, *Angew. Chem. Int. Ed.*, 2015, 54, 14372–14377.
- 22 H. S. Scott, A. Bajpai, K.-J. Chen, T. Pham, B. Space, J. J. Perry and M. J. Zaworotko, *Chem. Commun.*, 2015, 51, 14832–14835.
- 23 A. Cadiou, K. Adil, P. M. Bhatt, Y. Belmabkhout and M. Eddaoudi, *Science*, 2016, 353, 137–140.
- 24 L. T. Ngyen, K. K. LE and N. T. PHAN, *Chinese J. Catal.*, 2012, 33, 688–696.
- 25 A. R. Millward and O. M. Yaghi, *J. Am. Chem. Soc.*, 2005, 127, 17998–17999.
- 26 P. Nugent, V. Rhodus, T. Pham, B. Tudor, K. Forrest, L. Wojtas, B. Space and M. Zaworotko, *Chem. Commun.*, 2013, 49, 1606–1608.
- 27 O. Shekhah, Y. Belmabkhout, K. Adil, P. M. Bhatt, A. J. Cairns and M. Eddaoudi, *Chem. Commun.*, 2015, 51, 13595–13598.
- 28 H. S. Scott, M. Shivanna, A. Bajpai, D. G. Madden, K.-J. Chen, T. Pham, K. A. Forrest, A. Hogan, B. Space, J. J. Perry IV and M. J. Zaworotko, *ACS Appl. Mater. Inter.*, 2017, 9, 33395–33400.

- 29 M. H. Mohamed, S. K. Elsaidi, T. Pham, K. A. Forrest, B. Tudor, L. Wojtas, B. Space and M. J. Zaworotko, *Chem. Commun.*, 2013, 49, 9809–9811.
- 30 S. K. Elsaidi, M. H. Mohamed, H. T. Schaef, A. Kumar, M. Lusi, T. Pham, K. A. Forrest, B. Space, W. Xu, G. J. Halder, J. Liu, M. J. Zaworotko and P. K. Thallapally, *Chem. Commun.*, 2015, 51, 15530–15533.
- 31 K.-J. Chen, Q.-Y. Yang, S. Sen, D. G. Madden, A. Kumar, T. Pham, K. A. Forrest, N. Hosono, B. Space, S. Kitagawa and M. J. Zaworotko, *Angew. Chem. Int. Ed.*, 2018, 57, 3332–3336.
- 32 S. Mukherjee, N. Sikdar, D. O’Nolan, D.M. Franz, V. Gascón, A. Kumar, N. Kumar, H. S. Scott, D.G. Madden, P.E. Kruger, B. Space and M.J. Zaworotko, *Sci. Adv.* 2019, 5.
- 33 D.G. Madden, D. O’Nolan, K.J. Chen, C. Hua, A. Kumar, T. Pham, K.A. Forrest, B. Space, J.J. Perry, M. Khraishah and M.J. Zaworotko, *Chem. Commun.*, 2019, 55, 3219–3222.
- 34 W. Liang, P.M. Bhatt, A. Shkurenko, K. Adil, G. Mouchaham, H. Aggarwal, A. Mallick, A. Jamal, and M. Eddaoudi, *Chem*, 2019, 5, 950–963.
- 35 X. Cui, Q. Yang, L. Yang, R. Krishna, Z. Zhang, Z. Bao, H. Wu, Q. Ren, W. Zhou, B. Chen and H. Xing, *Adv. Mater.*, 2017, 29, 1606929.
- 36 M. R. Tchalala, P. M. Bhatt, K. N. Chappanda, S. R. Tavares, K. Adil, Y. Belmabkhout, A. Shkurenko, A. Cadiau, N. Heymans, G. De Weireld, G. Maurin, K. N. Salama and M. Eddaoudi, *Nat. Commun.*, 2019, 10, 1328–1338.
- 37 J. Hedlund, O. Öhrman, V. Msimang, E. van Steen, W. Böhringer, S. Sibya and K. Möller, *Chem. Eng. Sci.*, 2004, 59, 2647–2657.
- 38 Y.-S. Li, F.-Y. Liang, H. Bux, A. Feldhoff, W.-S. Yang and J. Caro, *Angew. Chem. Int. Ed.*, 2010, 49, 548–551.
- 39 G. Lu and J. T. Hupp, *J. Am. Chem. Soc.*, 2010, 132, 7832–7833.
- 40 A. Bétard and R. A. Fischer, *Chem. Rev.*, 2012, 112, 1055–1083.
- 41 Y. Watanabe, T. Haraguchi, K. Otsubo, O. Sakata, A. Fujiwara and H. Kitagawa, *Chem. Commun.*, 2017, 53, 10112–10115.
- 42 L. Heinke, M. Tu, S. Wannapaiboon, R. A. Fischer and C. Wöll, *Micro. Meso. Mat.*, 2015, 216, 200–215.
- 43 H. K. Arslan, O. Shekhah, D. C. F. Wieland, M. Paulus, C. Sternemann, M. A. Schroer, S. Tiemeyer, M. Tolan, R. A. Fischer and C. Wöll, *J. Am. Chem. Soc.*, 2011, 133, 8158–8161.
- 44 V. Chernikova, O. Shekhah and M. Eddaoudi, *ACS Appl. Mater. Inter.*, 2016, 8, 20459–20464.
- 45 V. Chernikova, O. Shekhah, Y. Belmabkhout and M. Eddaoudi, *ACS Appl. Mater. Inter.*, 2020, 3, 6432–6439
- 46 A. Kumar, C. Hua, D. G. Madden, D. O’Nolan, K.-J. Chen, L.-A. J. Keane, J. J. Perry and M. J. Zaworotko, *Chem. Commun.*, 2017, 53, 5946–5949.
- 47 O. Shekhah, Y. Belmabkhout, Z. Chen, V. Guillermin, A. Cairns, K. Adil and M. Eddaoudi, *Nature Comm.*, 2014, 5, 4228.
- 48 M. Tagliabue, D. Farrusseng, S. Valencia, S. Aguado, U. Ravon, C. Rizzo, A. Corma and C. Mirodatos, *Chem. Eng. J.*, 2009, 155, 553–566.
- 49 D. O’Nolan, A. Kumar and M. J. Zaworotko, *J. Am. Chem. Soc.*, 2017, 139, 8508–8513.
- 50 J. Warfsmann, B. Tokay and N. R. Champness, *Cryst. Eng. Commun.*, 2020, 43, 2334–2343.
- 51 H. Bux, A. Feldhoff, J. Cravillon, M. Wiebcke, Y.-S. Li and J. Caro, *Chem. Mater.*, 2011, 23, 2262–2269.
- 52 J. Hromadka, B. Tokay, R. Correia, S. P. Morgan and S. Korposh, *Sensor Actuat B - Chem*, 2018, 255, 2483–2494.

- 53 J. Hromadka, B. Tokay, R. Correia, S. P. Morgan and S. Korposh, *Sensor Actuat B - Chem*, 2018, 260, 685–692.
- 54 J. Hromadka, B. Tokay, S. James, R. P. Tatam and S. Korposh, *Sensor Actuat B - Chem*, 2015, 221, 891–899.
- 55 A. Schejn, L. Balan, V. Falk, L. Aranda, G. Medjahdi and R. Schneider, *CrystEngComm*, 2014, 16, 4493–4500.
- 56 M. N. Shah, M. A. Gonzalez, M. C. McCarthy and H.-K. Jeong, *Langmuir*, 2013, 29, 7896–7902.

Supplementary information

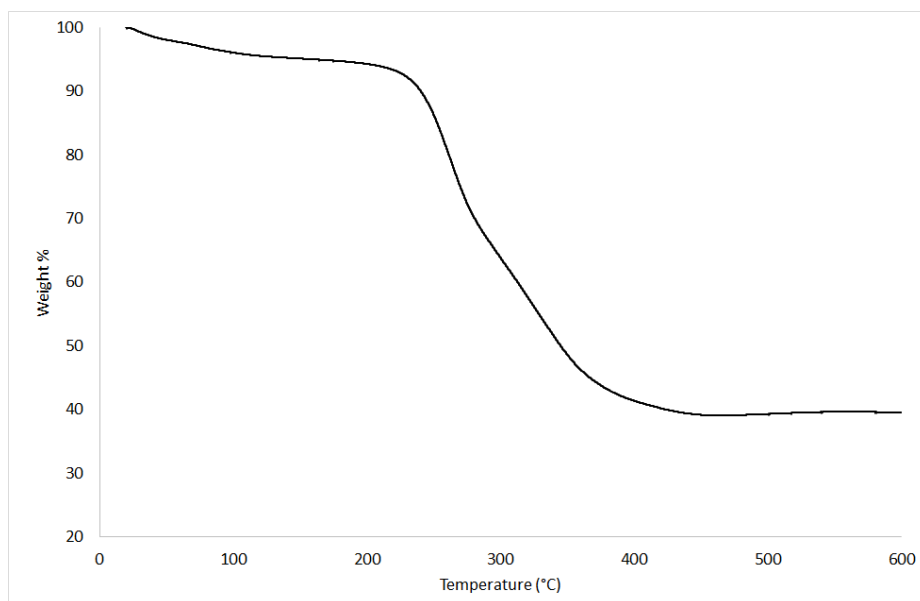
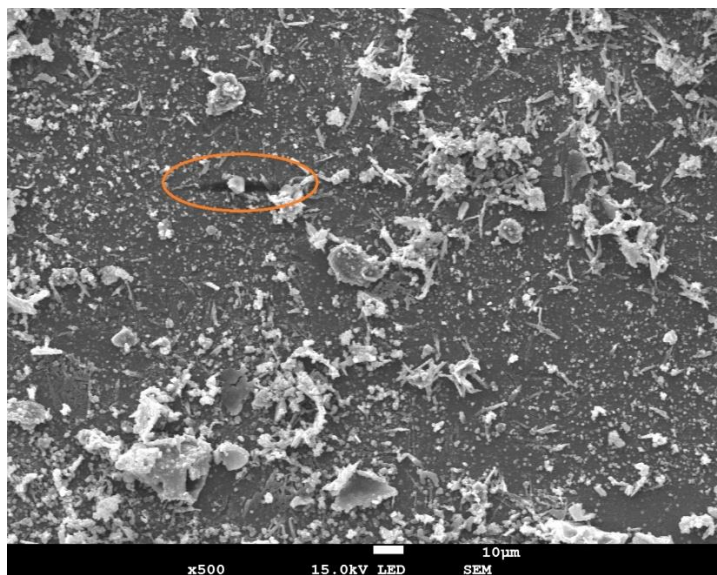


Figure S1: Thermal Gravimetric analysis of TIFSIX powder prepared in DMF at 85 °C for 15 h.



FigureS2: Low magnification SEM image of glass covered by TIFSIX in DMF at 85 °C for 5 h via in-situ coating. The surface is mostly covered, but some small cracks (orange marking) are visible. At the top of the TIFSIX coating, larger needle-shaped and clustered particles are visible, which resemble particles known from powder synthesis.

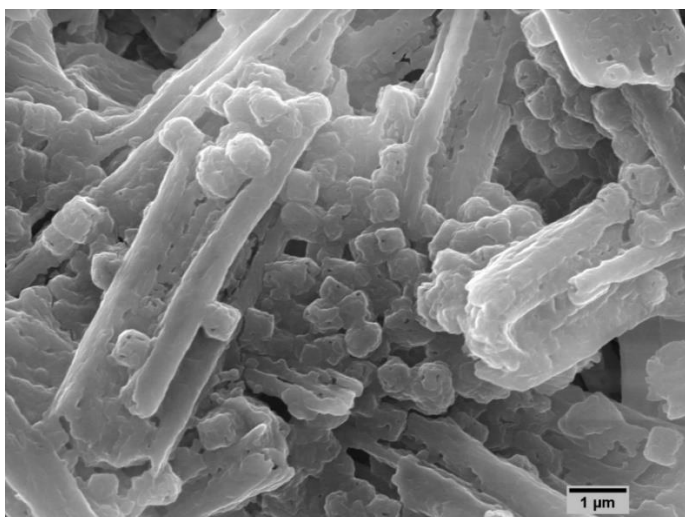


Figure S3: High magnification SEM image of glass slide covered by TIFSIX in DMF at 85 °C for 15 h via in-situ coating. Cubic shaped particles, which fuse to larger needle-shaped particles, are visible. They have 308 ± 107 nm edge length comparable to the 5 h sample but the edges are less distinctive and more intergrown, most likely due to the longer reaction time.

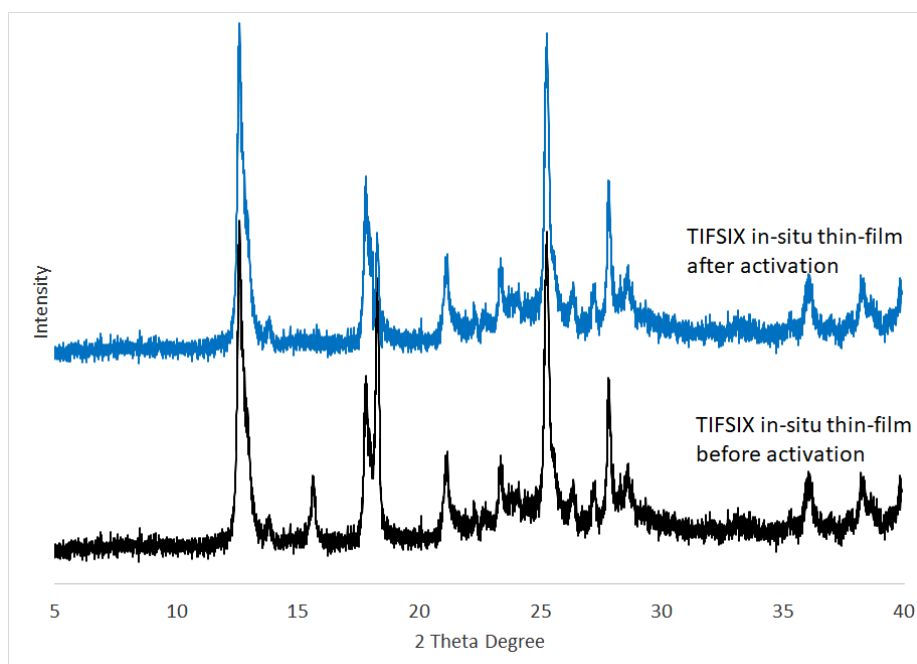


Figure S4: XRD patterns of TIFSIX films by in-situ coating at 85°C for 5 h before (black) and after (blue) activation by solvent exchange in MeOH and heating at elevated temperature. During the activation, the intensity of some impurity peaks (e.g. at 15.7° and 18.2°) could be reduced.

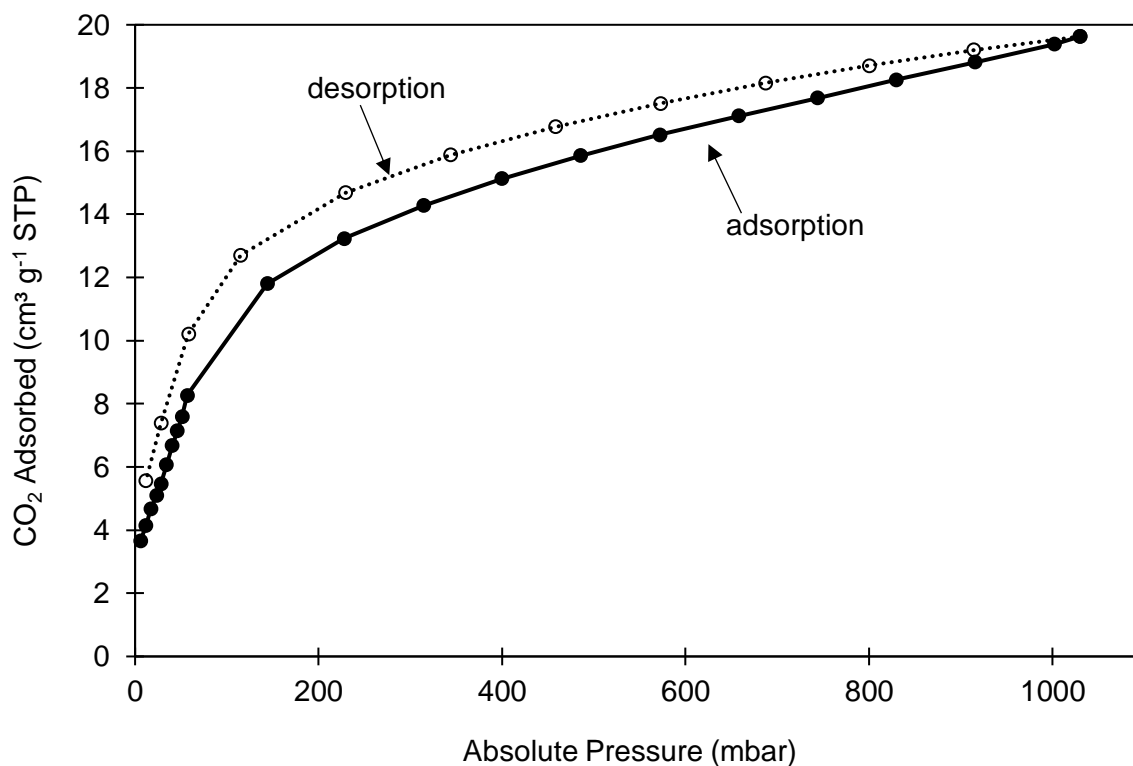


Figure S5: CO₂ isotherms of TIFSIX powder, collected from the bottom of the vessel after in-situ film formation.

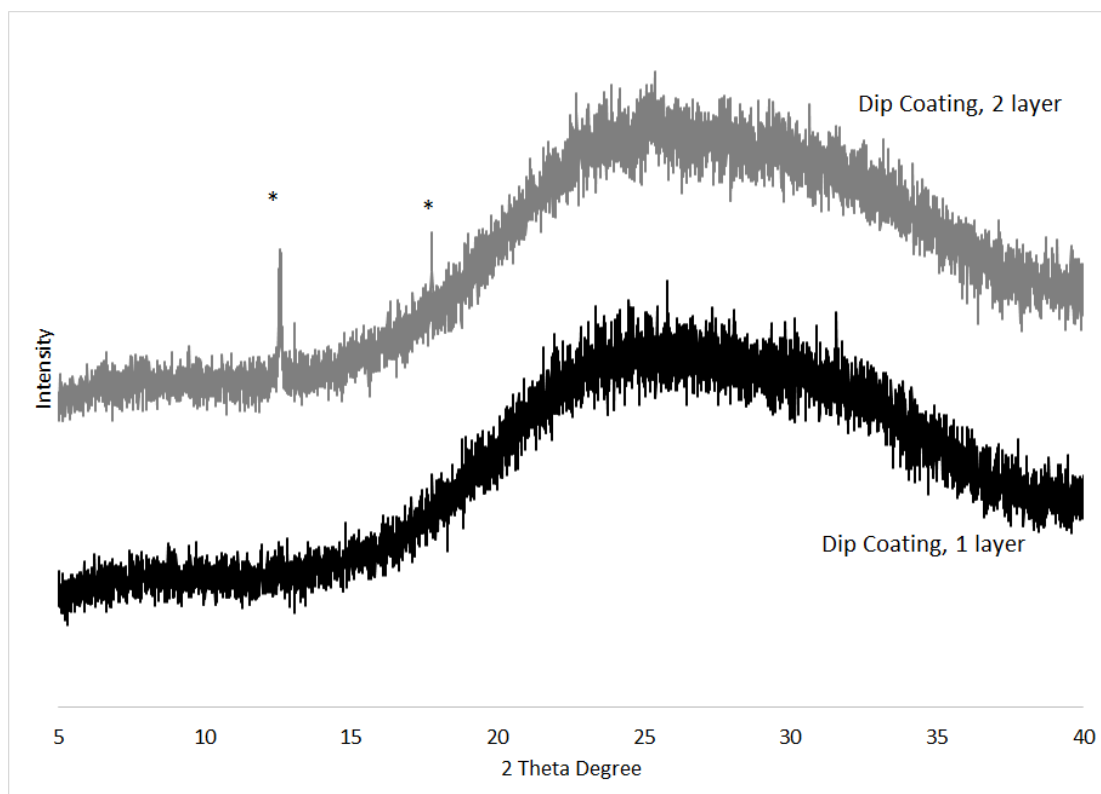


Figure S6: XRD patterns of glass slides covered with TIFSIX with one layer (black) and two layers (grey) by dip-coating.

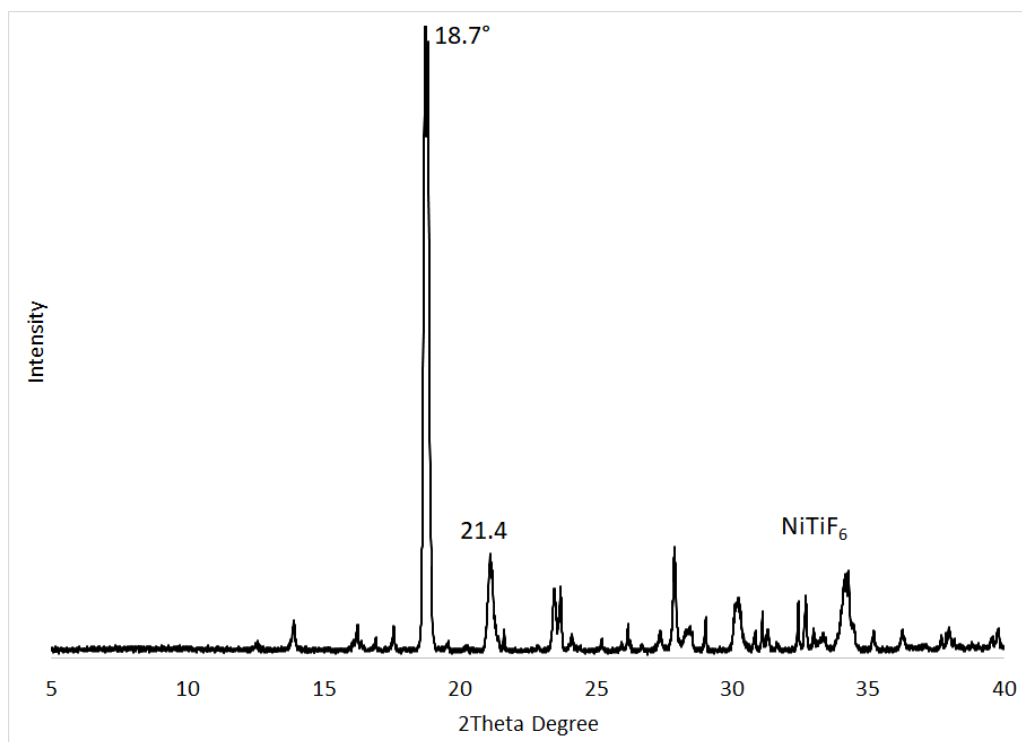


Figure S7: XRD pattern of the starting material NiTiF_6 .

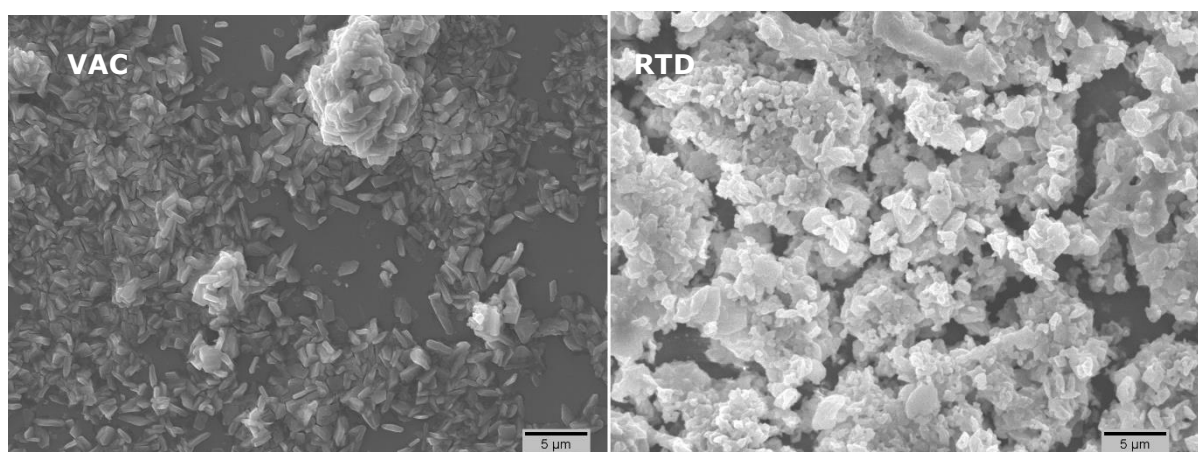


Figure S8: SEM images of films on the glass slides, covered by vapour-assisted conversion (VAC) and rapid thermal deposition (RTD).